Journal of CO2 Utilization 68 (2023) 102370

Contents lists available at ScienceDirect

Journal of CO2 Utilization

journal homepage: www.elsevier.com/locate/jcou

Cyclic performance in CO_2 capture-methanation of bifunctional Ru with different base metals: Effect of the reactivity of COx ad-species

Enrique García-Bordejé [a,*], Ana Belén Dongil [b], Jorge Moral [b], José M. Conesa [b,c], Antonio Guerrero-Ruiz [c,d], Inmaculada Rodríguez-Ramos [b,d]

[a] Instituto de Carboquímica (ICB-CSIC), Miguel Luesma Castán 4, E-50018 Zaragoza, Spain
[b] Instituto de Catálisis y Petroleoquímica (CSIC), 28049 Madrid, Spain
[c] Departamento de Química Inorgánica y Química Técnica, UNED, 28040 Madrid, Spain
[d] Grupo de Diseño y Aplicación de Catalizadores Heterogéneos, Unidad Asociada UNED-CSIC (ICP), Spain

ARTICLE INFO

Keywords:
CO_2 capture and methanation
Alkaline metals
Ru catalyst
TPSR
Dual functional materials

ABSTRACT

Bifunctional materials based on Ru nanoparticles and an alkaline metal (K, Na or Ba) have been scrutinized for several cycles of CO_2 capture and subsequent methanation at different temperatures from 250 ºC to 450 ºC. The optimum performance in terms of stable cyclic operation, amount of captured CO_2 and relevant methane productivity was attained at different temperature window for each material. For the materials here prepared, the limiting lower operation temperature of stable cyclic performance was determined by the methanation kinetics, which depended on reactivity of COx ad-species captured with each alkaline metal. The highest activity was found with Ba-containing materials, which exhibited a stable and relevant cyclic CH_4 productivity at 250 ºC, being one of the lowest operation temperatures reported for a dual functional material to date. This material exhibited stable cyclic performance also in the presence of O_2 and H_2O, although the CH_4 productivity decreases slightly and reversibly compared to that using CO_2 containing gas free of O_2 and H_2O.

1. Introduction

CO_2 emissions have been increasing in the last few decades due to anthropogenic causes leading to global warming [1]. In this scenario, the Paris Agreement sets out a global framework to limit global warming to well below 2 °C and pursuing efforts to limit it to 1.5 °C [2]. To reach this target, intense research efforts have been devoted to carbon capture and storage (CCS) and carbon capture and utilization (CCU). Post-combustion effluents contain CO_2 plus a complex mixture of other components (H_2O, O_2, sulphur and nitrogen oxides). Therefore, the conversion cannot be performed directly and CO_2 needs to be captured previously. Chemical absorption using solvents such as ethanolamine seems more suitable than adsorption for CO_2 capture from post-combustion gases, which are emitted at low pressure [3]. Nevertheless, the steps of thermal regeneration of solvent and CO_2 purification are energy intensive, and the rates of solvent degradation and equipment corrosion can also penalise this process [4]. Physical adsorption is more suitable for CO_2 capture at high pressure and low temperatures and yields less waste during cycling. However, the used adsorbents have lower selectivity to CO_2 and lower adsorption rate. Solid sorbents such as alkaline metal oxides can reversibly and selectively capture CO_2 by forming carbonates [5,6]. This process is carried out at intermediate temperatures (200–400 ºC), matching the temperature of post-combustion flue gases. Subsequently, the captured CO_2 can be utilized to produce fuel by reacting with renewable hydrogen, and in turn regenerating the adsorbent for next cycle. In this way, CO_2 utilisation is coupled with the storage of the intermittent renewable energy to produce a stable and transportable energy carrier such as methane. The process is also known as combined CO_2 capture and methanation (CCCM) [7]. The methane can be used as fuel for mobility, residential sector, power generation or raw material in industry.[8] Different process configurations can be devised to perform CCCM. One way is using two separate units with different gas feeds, i.e. one unit for the periodic adsorption and desorption of CO_2 and the other for the methanation [9–12]. In this configuration, each unit has different operating conditions which can be optimised independently but it is energy and time intensive due to temperature swings. CCCM can be also performed in one unique unit containing both the capture material and the

* Corresponding author.
E-mail address: jegarcia@icb.csic.es (E. García-Bordejé).

https://doi.org/10.1016/j.jcou.2022.102370
Received 5 September 2022; Received in revised form 28 November 2022; Accepted 11 December 2022
Available online 19 December 2022

methanation catalyst with periodic swinging of the gas feed. This process will also allow for continuous operation using two parallel reactors working in tandem. In this process, both CO_2 capturing solid and methanation catalyst can be either physically separated [13] or a single homogeneous solid can feature both functionalities. This latter type of solid is denoted as "dual functional material (DFM)", which usually consists of two different metals in very intimate contact: an alkaline metal as CO_2-absorbing material and a transition metal (Ni,Ru) as methanation catalyst on a high surface area support such alumina. Both absorption and methanation reactions operate in the same temperature window (300–500 ºC) enabling isothermal operation for both steps, avoiding temperature swings, and also matching the temperature of post-combustion flue gases. The main reactions occurring in the two steps for the case of Na_2O as capture material can be outlined as follows [14]:

CO_2 capture step:

$$Na_2O + CO_2 \rightarrow Na_2CO_3 \quad (1)$$

Hydrogenation/regeneration step:

$$Na_2CO_3 + 4\ H_2 \rightarrow CH_4 + Na_2O + 2\ H_2O \quad (2)$$

$$Na_2CO_3 + H_2 \rightarrow CO + Na_2O + H_2O \quad (3)$$

It is claimed that the close proximity between the two functionalities (capture and methanation) results in enhanced performance for the regeneration/methanation step [7,14]. On the one hand, because the close proximity between the two functions favours the spill-over of H_2 to the captured CO_x ad-species[15] and concomitantly the transport of desorbed CO_2 to the metal catalytic sites [16,17]. On the other hand, since the CO_2 desorption is endothermic and the methanation is exothermic, the heat transfer is faster and both reactions can be energetically balanced choosing the suitable adsorbent and reaction conditions. Moreover, this process avoids the high energy consumption of conventional CO_2 separation and purification needed when the process is carried out in two separate units. For all the reasons mentioned heretofore, DFMs contribute remarkably to process intensification. However, since the process of CO_2 desorption and conversion are coupled, DFMs introduce other challenges in terms of material preparation and process parameters design for an optimum operation.

Intense effort has been devoted recently to optimise catalyst formulations and preparation strategies. Farrauto et al. pioneered the research on DFMs for CCCM. They started preparing DFMs varying both the Ru loadings (1–10 wt%) and CaO loading (1–10 wt%) on γ-Al_2O_3 [18]. The best catalyst was that with intermediate Ru loading (5 wt%). The same group performed a screening of different active phases for methanation (Ru, Rh, Pt, Pd, Ni, Co) and adsorption (MgO, K_2O_3, Na_2CO_3) [19,20]. They performed both CO_2 capture and conversion at 320 ºC, finding that Ru provided better performance than Ni and the best alkaline among those tested was Na. Some authors used other metals such as FeCrCu [21] or Cu [22] to produce selectively syngas instead of CH_4. In cycles of CO_2 capture and methanation, the temperature of regeneration (CO_2 release) and methanation should match. $CaCO_3$ decomposition temperatures is around 700ºC [6], being incompatible with temperatures of methanation which are much lower (250–400 ºC) since at higher temperatures the reverse-water gas shift (RWGS) reaction prevails, leading to CO. Carbonates formed with Na have less stability than those with Ca. Consequently, DFMs based on Ni-Na produced more CH_4 at lower temperature than Ni-Ca as corroborated by Bermejo-López et al. [23]. For Ni-Ca the CH_4 production was maximized at 400 ºC, which is a relatively high temperature entailing massive energy consumption. The order of impregnation of metal also affects the performance. Using the combination CaO:Ru, Duyar et al. [18] found that impregnation of Ru on CaO/γ-Al_2O_3 resulted in better performance compared to materials where CaO is impregnated on Ru/γ-Al_2O_3. Kuramoto et al. [24] tested Ni on alumina plus several alkaline metals (K, Na, Ca) for CCM. Among the tested materials, Ni/Na-γ-Al_2O_3 showed the highest activity for integrated CCM. The Ni-based DFM exhibited a high CO_2 conversion exceeding 90%, even when 20% O_2 was present in CO_2-containing combustion flue gas. However, the temperature of testing was relatively high (450 ºC) and it would be desired to operate the process at lower temperatures for energy saving. Elsewhere, Urakawa et al. [25] studied DFM based on Ni on ZrO_2 promoted with K- or La- in the operating temperature range 250–450 ºC. La-doped catalyst was more efficient for methanation but a high proportion of unreacted CO_2 was released because the catalyst was not sufficiently active at lower temperatures. To have fast methanation kinetics and regenerate the catalyst for subsequent cycle, the processes are usually carried out at temperatures above 300 ºC for K and Na based DFMs [20] Other alkaline that has been used in DFM is Li [26]. Li-Ru/Al_2O_3 provided better performance than its counterparts with K or Na, showing cyclic CH_4 production at low temperature of 230 ºC, which is the lowest temperature reported for DFMs. Working at lower temperatures would reduce the energy requirements for heating gases and would avoid hot spots. Low temperatures would be even more crucial when the direct CO_2 capture from air (DAC) is addressed as proposed in the literature [14,24,27] since air should be heated during the long adsorption times required for this very diluted CO_2 source. The operation temperature of DFM is determined by the optimum methanation kinetics. Using state-of-the art DFM, 320ºC is chosen as optimum temperature [14]. Methanation can occur at lower temperatures but kinetics is slow with current DFMs. Therefore, it is a challenge to find novel DFMs able to be regenerated and with fast methanation kinetics at temperatures lower than 250 ºC. Since the temperature affects the adsorption/reaction thermodynamics and kinetics, the operation temperature should be optimized on an individual basis for each DFM type. Only a few works perform parametric studies optimising the temperature for several cycles [28,29] These works found that the best temperatures were 320 ºC and 300 ºC for the optimised catalyst 5%Ru-10%CaO/ γ-Al_2O_3 [28] and 5% Ru-6.1% Na_2O/γ-Al_2O_3,[29] respectively.

As explained above, different metals of group I and group II have been compared as capture component for DFMs[23,24,30] Among the metals tested, heavier group II metals such as Ba are comparatively scarcely investigated in existing literature. To the best of our knowledge, there is only one group reporting Ba as CO_2 capture material in DFM to date [31,32]. This works indicate that BaO is less effective than other alkaline metals because it forms stable carbonates at temperatures from 350 ºC to 500 ºC,[31] thus avoiding regeneration in subsequent cycle. However, the performance at lower temperatures was not explored. Many works do not address the long-term stability and the CH_4 productivity is only reported for one or few cycles of capture and reduction [17,23,25,32]. Some work performed up to ten cycles and the performance degrades with the number of cycles, which is attributed to sintering of alkaline metal [33]. Therefore, for practical application, it is crucial to check the stability in cyclic tests at different temperatures.

Herein, we have compared the performance of DFMs consisting of one methanation metal (Ru) and a CO_2 capture material. As capture material, we have also scrutinized the less explored barium besides the widely used alkaline metals (Na, K). We study the cyclic performance as a function of the operation temperature in the range from 250 ºC to 450 ºC. DFMs are usually tested only at temperatures above 300 ºC. To assess the cyclic stability, at least 6 cycles have been carried out at each temperature for all DFMs. Finally, a selected catalyst and temperature has been tested in the cyclic capture of CO_2 using a gas containing also H_2O and O_2. The characterisation by different techniques shed some light into the reaction mechanism and the reasons of the dependence of the cyclic stability and reaction kinetics on the type of base metal.

2. Experimental

2.1. Catalyst preparation

Alumina support was prepared from Pural (SASOL) calcined at 500 ºC in air. The chemicals precursor for Ru metal was $Ru(NO_3)_3NO$ (Alfa Aesar). As precursor of the alkaline metals K_2CO_3, $NaNO_3$ and $Ba(NO_3)_2$ (Sigma-Aldrich) were used.

The DFM were prepared by successive incipient wetness impregnation first of the alkaline precursor and second of Ru precursor. That means that in the impregnation the precursor was diluted in the volume of water corresponding to the pore volume of the solid. The alkaline metal precursor was weighted to yield a final loading of 10 wt% respect to γ-alumina weight, diluted in water and impregnated on alumina by incipient wetness impregnation. After drying at 110 ºC, the material was calcined at 500 ºC under N_2. Subsequently, the amount Ru precursor was weighted to set a 3 wt% loading with respect to alumina. After drying at 110 ºC, the material was calcined at 500 ºC under N_2 flow for 1 h and subsequently reduced under H_2 flow at the same temperature for 1 h.

2.2. Cyclic testing

The testing in cycle of CO_2 adsorption and reduction was carried out in a continuous-flow 6 mm-outer-diameter quartz reactor inside a vertical furnace equipped with a temperature controller (Eurotherm). The amount of monometallic catalyst used in the catalytic tests was 50 mg. For the bimetallic catalyst, the amount of catalyst was adjusted to have the same Ru weight than the monometallic catalyst. Particle size was between 20 and 53 μm (625–270 mesh). Subsequently, the catalyst was diluted with the double volume of SiC and placed inside the reactor forming a packed bed of 2 cm length with a thermocouple inside the bed. The high thermal conductivity of SiC, particle size < 100 μm and the small bed diameter guarantees that the temperature is uniform throughout all the bed without hot spots. The temperature of the bed is exactly that measured by the thermocouple. This bed gives rise to 16 Pa pressure drop. The reaction temperature was controlled with a thermocouple inside the catalytic bed. Prior to cyclic tests, the catalyst was heated to 500 ºC in N_2 flow using a heating rate of 10 ºC min^{-1} and it was reduced with H_2 (60 mL min^{-1}) at 500 ºC for 1 h. The reactor was allowed to cool down until the temperature of the cyclic testing). The cycles consist of two stages: *(i)* first, flowing 60 mL/min of 5% CO_2 in Ar and *(ii)* second, flowing 60 mL/min of 5% H_2 in Ar. The times of each stage were varied for the different experiments (between 2 and 10 min) until steady state was reached. Between the two stages, the reactor was swept with 57 mL/min Ar flow for 5–25 min until CO_2 signal stabilisation. Six or more capture/reduction cycles were performed for all the materials. Gas analysis was performed using a Pfeiffer vacuum mass spectrometer. The following m/z signals were recorded in mass spectrometer: 2, 16, 18, 28, 40, 44. The signals of the gases were calibrated considering the baseline of Ar and the fragmentation pattern of each mass. The main m/z signals used for each gas were 2 (H_2), 16 (CH_4), 18 (H_2O), 28 (CO), 40 (Ar) and 44 (CO_2). The concentration of CO was calculated subtracting the contribution of CO_2 from $m/z = 28$. The concentration of CH_4 was calculated subtracting the contribution of CO_2, CO and H_2O from $m/z = 16$. The correct calibration of the mass spectrometer was double checked analyzing the gases using a calibrated Agilent Micro GC 3000 A.

2.3. Catalyst characterization

The catalysts were characterized by transient techniques, namely, temperature-programmed desorption of pre-adsorbed CO_2 (CO_2-TPD) and temperature programmed surface reaction (TPSR). These experiments were conducted in the same set-up as catalytic testing. The purpose of CO_2-TPD experiments is to quantify the CO_2 chemisorbed at 300 ºC. To this end, the catalyst was heated to 500 ºC at a heating rate of 10 K min^{-1} in inert gas. At this temperature, the catalyst was reduced with 100 mL min^{-1} of H_2 mixture for 1 h. Subsequently, the temperature was set at 300 ºC and 60 mL min^{-1} of CO_2 was flushed for 1 h. The gas was switched to 60 mL min^{-1} Ar and the reactor was allowed to cool down to room temperature. Ar flow was kept constant overnight to remove all weakly physisorbed CO_2. Then the gas was adjusted to 60 mL min^{-1} of Ar and, when the signal of the mass spectrometer was stable, the temperature was increased to 500 ºC at a rate of 10ºC per minute while monitoring the desorbed gases, mainly CO_2.

The main purpose of TPSR experiments is to determine the temperature at which CH_4 starts to evolve from reaction of H_2 gas with CO_2 previously adsorbed on the catalyst. To this end, the catalyst was heated to 500 ºC at a heating rate of 10 K min^{-1} in inert gas. At this temperature, the catalyst was reduced with 100 mL min^{-1} of H_2 mixture for 1 h. Subsequently, the catalyst was cooled down to 50 ºC under Ar. When this temperature is reached 60 mL mi of CO_2 was flushed for 1 h. Then, the gas was switched to 60 mL min^{-1} of 5% H_2 in Ar and kept until the signal of the mass spectrometer was stable. Subsequently, the temperature was increased to 500 ºC at a rate of 10ºC per minute while monitoring the desorbed gases, mainly CH_4.

The XEDS-mapping analyses were performed in STEM mode with a probe size of ~1 nm using the Oxford INCA Energy 2000 system detector. The samples were ground until powder and a suspended in ethanol solution using an ultrasonic bath. Then some drops were added into the copper grid with carbon coated layers (Aname, Lacey carbon 200 mesh) leaving to dry at room temperature to evaporate ethanol before introducing in the microscope.

Structural properties of the catalyst were determined by X-ray diffraction (XRD), XRD profiles were obtained in Polycristal X´Pert Pro PANalytical diffractometer using Ni-filtered Cu Kα radiation ($\lambda = 1.54$ Å, 45 kV and 40 mA) with a 0.04° step and the Diffract-EVA software was used for the phases identification.

The X-ray photoelectron spectra of the samples after reaction were recorded using an Omicron spectrometer refurbished by SPECS, equipped with a PHOIBOS 100 R4 analyzer and a monochromatic X-ray source (Mg Kα) operated at 75 W, with a pass energy of 30 eV and an energy step of 0.050 eV. Each sample was pressed into a small pellet, placed in the sample holder and degassed in the chamber for 6–8 h to achieve a dynamic vacuum below 10^{-8} Pa before analysis. The spectral data for each sample were analysed using CASA XPS software. The binding energy is referenced to the Al 2p line at 74.7 eV. The relative concentrations and atomic ratios were determined from the integrated intensities of photoelectron lines corrected for the corresponding atomic sensitivity factor. Carbon elemental analysis was carried out directly in a Flash 1112 de Thermofisher.

3. Results and discussion

3.1. Testing in cycles of CO_2 capture and reduction

Herein, the cyclic performance in CO_2 capture and subsequent hydrogenation has been assessed for at least 6 isothermal cycles at different temperatures ranging from 250 ºC to 450 ºC and using the different materials prepared in this work. As example, Fig. 1 shows representative cycles of CO_2 capture and reduction at 300 ºC for a monometallic and the three bimetallic materials. The cyclic testing at other temperatures for all DFMs are shown in supplementary information (Figs. S1-S3 of supplementary material). In the stage of feeding CO_2 in Ar, CO_2 is initially captured on the storage material. We have to note that we used an excess of CO_2 to ensure the saturation of the capture material. Therefore, this work has been focused on the comparison of the material capacity but not on the CO_2 capture efficiency that should be a next step because high efficiency is necessary for industrial application. In order to emit a CO_2-free gas, it would be only necessary to increase the amount of DFM or decrease the flow rate of CO_2 containing gas. Concomitantly to CO_2 feeding, there is a release of other gases such as CO, H_2O and minor

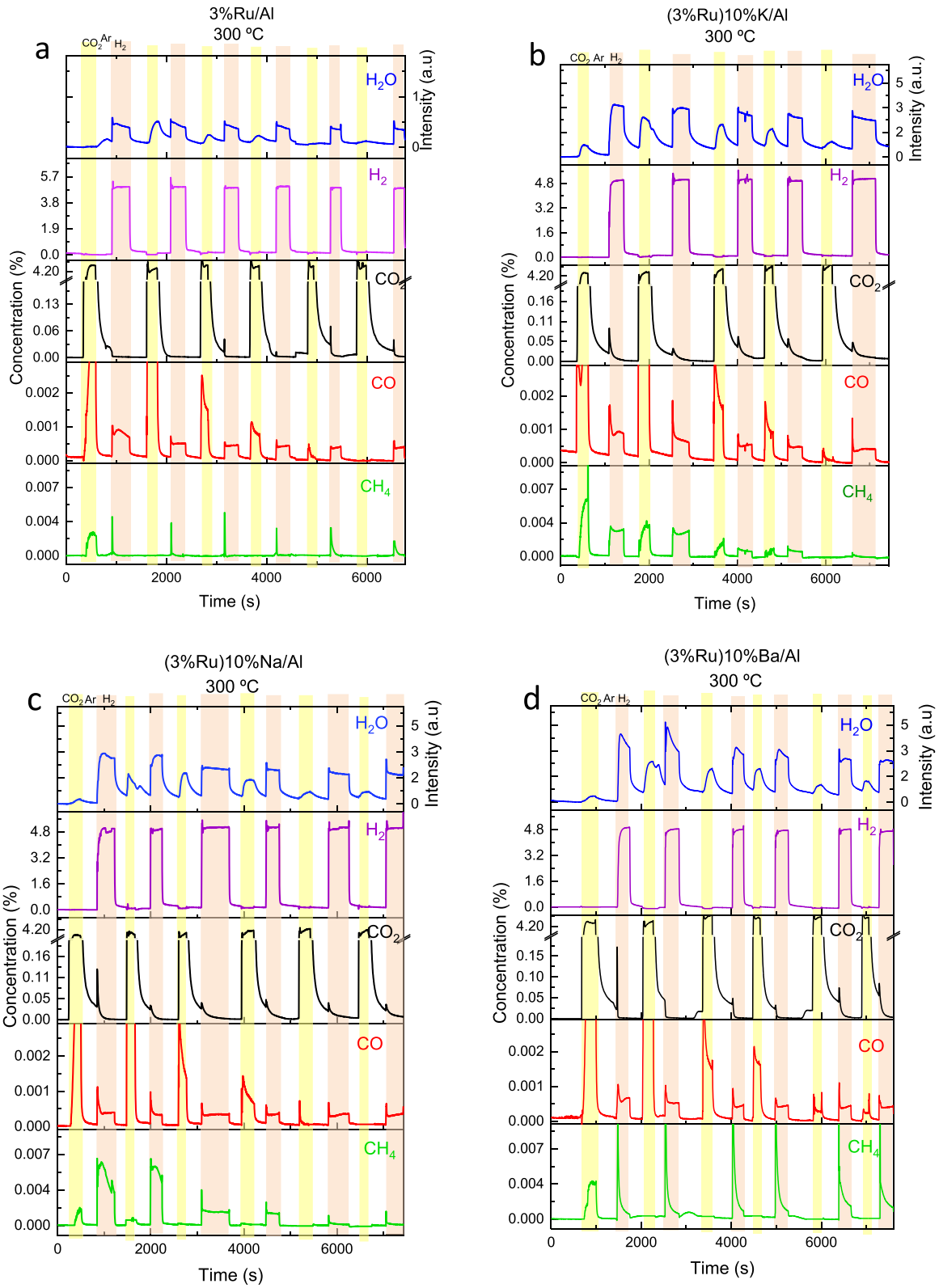

Fig. 1. Representative cycles CO_2 capture and conversion using Ru-based catalysts with and without different alkaline metals at 300 ºC: (a) monometallic 3% Ru/Al; (b) (3%Ru)10%K/Al; (c) (3%Ru)10%Na/Al; (d) (3%Ru)10%Ba/Al. CO_2 capture step is shadowed in yellow while reduction step is shadowed in red.

amount of CH_4. These gases are the products of CO_2 gas reduction by the hydrogen atoms that remain chemisorbed on Ru metal after previous stage under H_2 containing gas. The main product in this oxidation stage is CO, which is formed primarily via r-WGS reaction between CO_2 and residual surface hydrogen [32]. The concentration of the released gases during CO_2 feeding stage decreases as the number of cycles increase. The reason could be that initially the catalyst contains the highest amount of -H species because it has been reduced previously at 500 ºC in H_2. In the following reduction stage, the catalyst is reduced/regenerated with 5% H_2 in Ar at temperatures lower than 500 ºC and shorter time, e.g. in

Fig. 1 the catalyst is regenerated at 300 ºC during 5 min. It can be envisaged that the amount of -H chemisorbed in reduction stage decreases as the number of cycles increases. After a few first conditioning cycles, the concentration of gases evolved during CO_2 feed tend to stabilise to their minimal value.

In the reduction stage, captured CO_2 is converted with the evolution of CH_4, CO, H_2O and unreacted CO_2·H_2O is formed by reaction of H_2 with oxygen coming from CO_2 dissociation in previous step. The amount of released CO_2 is minor and decreases to zero as reaction temperature increases (Supplementary Figures and Table S1). CO formation is higher in the first cycles and its intensity decays as the cycle number increases. In contrast, the intensity of CH_4 peak either decays to negligible values when the DFM performance degrades (Fig. 1b,c) or it is almost constant for all the cycles indicating a stable cyclic CH_4 production (Fig. 1d). In this latter case, this results in a CH_4 selectivity rise as the number of cycles increases.

Fig. 2 shows a magnification of the reduction stage corresponding to 2nd cycle of Fig. 1 for the different catalyst. For the monometallic 3% Ru/Al_2O_3 catalyst, there is some spike in the CO, CH_4 and H_2O evolution upon H_2 switching on. CH_4 concentration drops to zero in less than 20 s. However, CO concentration remains constant and H_2O decays slowly during 400 s. The absence of alkaline metal suggest that the prolonged minor CO production comes from species stored in the Al_2O_3 support. Compared to monometallic 3%Ru/Al_2O_3 catalyst, for the alkaline-containing materials, there is also a spike in CH_4 production but it takes longer to drop to zero. For the monometallic Ru catalyst, CO_2 can adsorb both on the metal and on the -OH of Al_2O_3 support [16]. When the alkaline is introduced an additional adsorption occurs, which is reported as bicarbonates and bidentate carbonates [16] or formates [22]. For Ba-containing material CH_4 evolution last more than 40 s while for K and Na-containing materials the CH_4 production is sustained for the whole duration of the reduction stage (~ 400 s). The shorter duration of the release of CH_4 for Ba-containing material than for K and Na-containing ones may be attributed to the higher amount of stored CO_2 in K and Na containing materials than in Ba-containing ones as shown in CO_2-TPD below. For K and Na containing materials there is also a minor release of unreacted CO_2, while no CO_2 at all is observed for Ba-containing material.

We quantified the CH_4 released in the first 100 s after the onset of the CH_4 spike. This was done by integrating the area under the mass spectrometer signal. The quantification of CH_4 and CO gases produced per gram of DFM as a function of the cycle number for the different temperatures and DFMs is displayed in Fig. 3.

The CO concentration decreases with the number of cycles (Fig. 3b,d, f) as explained for Fig. 1 description. The first cycles are conditioning cycles and are not relevant to the cyclic performance. After several cycles, the CO concentration stabilises at a small value (0.00–0.06 mmol g^{-1}). On the other hand, the CH_4 productivity depends on the temperature and on the type of DFM. The selectivity to CH_4 for all catalyst is above 80% when stable cyclic performance is achieved. At 300 ºC, for K and Na based materials the CH_4 productivity decays progressively with the cycle number to negligible values in 5th cycle. Other authors also reported degradation with the cycle number at 300ºC for physical mixtures of Na sorbent and Ru catalyst [10]. In contrast to our work, aging studies performed with 5%Ru, 6.1%Na_2O/γ-Al_2O_3 tablets by other authors [29] showed stable cyclic performance at 300 ºC or slow very deactivation at 320 ºC under industrially relevant conditions [34]. This suggest that the performance is very sensitive to the metal loadings and preparation method and we have to perform further optimisation of the formulation of our catalyst. The measurement of temperature is also very critical since methanation is an exothermic reaction and hot spots can occur. In our experiments the use of a thermal conductive diluting particles (SiC) in the bed where the thermocouple is inserted guaranties the measurement of the true temperature [35].

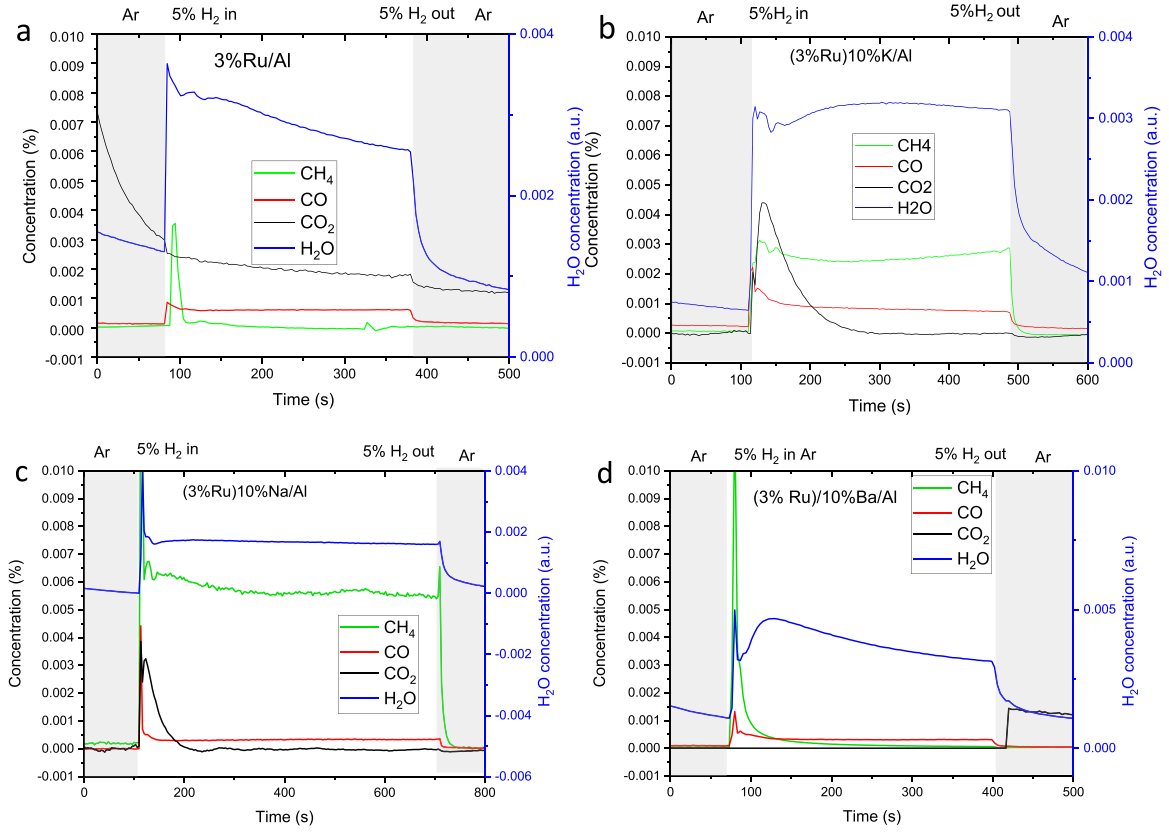

Fig. 2. Gas composition in 2nd cycle of reduction stage (5% H_2 in Ar) for different catalysts at 300 ºC: (a) 3%Ru/Al; (b) (3%Ru)10%K/Al; (c) (3%Ru)10%Na/Al; (d) (3%Ru)10%Ba/Al.

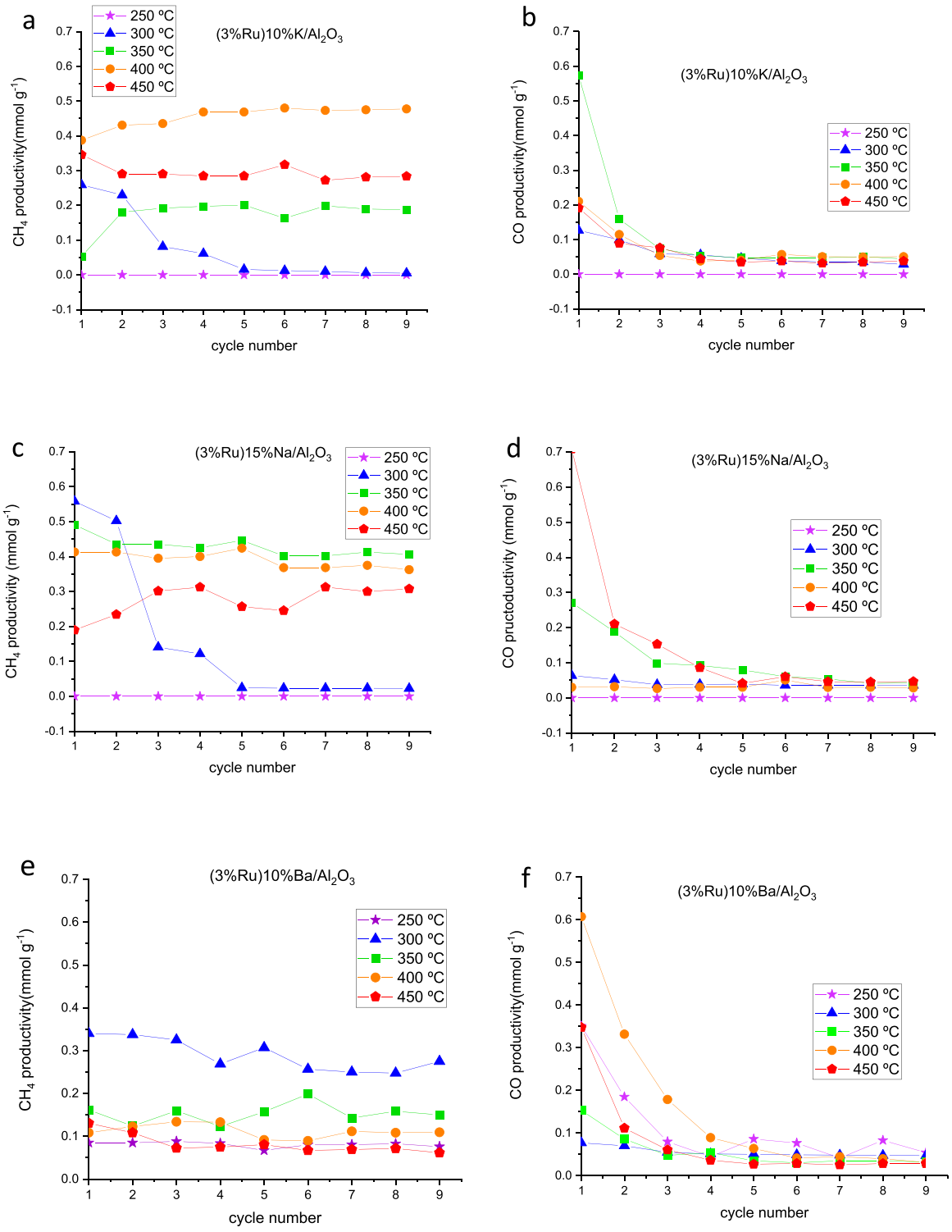

Fig. 3. Productivity of CH_4 (a,c,e) and CO (b,d,f) during the first 100 s of the reduction stage in each cycle for (3%Ru)10%K/Al (a,b), (3%Ru)10%Na/Al (c,d) and (3%Ru)10%Ba/Al (e,f).

On the other hand, the Ba-based material here prepared provided a stable CH_4 productivity ~0.28 mmol g^{-1} at 300 ºC after a small decay in the first cycles. For operation temperatures equal or above 350 ºC, the CH_4 productivity is almost constant with the cycle number for all the prepared materials. The decrease of CH_4 productivity with cycle number for K and Na based materials at 300 ºC can be attributed to the incomplete regeneration of capture material due to the building up of carbonated species that are stable at this temperature in H_2.[36] Since the alkaline oxide is not completely regenerated for the next CO_2 capture stage, it loses CO_2 capacity as the cycle number increases. Apparently, for temperatures equal or above 350 ºC, most carbonated species become unstable and are able to react with H_2, regenerating properly the capture material. For the temperatures of stable cyclic performance, CH_4 productivity does not follow a direct dependence with the temperature. The temperature of maximum CH_4 productivity is different for each material, namely 400 ºC (0.48 ± 0.03 mmol g^{-1}), 350 ºC (0.41

± 0.04 mmol g^{-1}) and 300 °C (0.28 ± 0.03 mmol g^{-1}) for (3%Ru)10% K/Al, (3%Ru)10%Na/Al and (3%Ru)10%Ba/Al, respectively. The variation of CH_4 productivity with the temperature for the same DFM is difficult to rationalise because the several processes involved in the stages of CO_2 capture and reduction have different dependences with the temperature. The CO_2 adsorption is favoured at lower temperatures while COx methanation kinetics is favoured at higher temperatures. Moreover, the kinetics of reduction of the RuOx active phases are also favoured at higher temperatures. It is remarkable that the CH_4 productivity for Ba-containing DFM is significantly higher at 300 °C than at higher temperatures. Other authors found that CO_2 is strongly adsorbed on supported BaO at temperatures from 350 °C to 500 °C in the form of carbonates with a very high thermal stability [31]. These species could not be completely hydrogenated when exposed to 4% H_2/He at 350 °C. This would explain the substantially poorer CH_4 productivity found here for temperatures of 350 °C and above compared to that for 300 °C, at which these stable Ba carbonates are not presumably formed.

Since the performance of (3%Ru)10%Ba/Al at the lowest temperature of 300°C was stable while keeping a high value of CH_4 productivity, we decided to perform the cyclic test at a lower temperature of 250 °C. At this temperature, we found that, while K and Na based DFMs provided negligible CH_4 productivity, (3%Ru)10%Ba/Al provided a stable CH_4 productivity of 0.08 ± 0.005 mmol g^{-1} during the 10 tested cycles as displayed in (Fig. 4 and S5 a). Subsequently, other 10 cycles were performed introducing in the feed 11% H_2O and 4.5% O_2 along with 5% CO_2 in Ar (Fig. 4 and S5b). The CH_4 productivity is slightly suppressed down to 0.05 ± 0.003 mmol g^{-1} (Fig. 4) because less CO_2 is captured probably due to competitive adsorption with water vapor. However, the CH_4 productivity remains stable from cycles 11–20 and the effect is reversible because the material recovers its initial CH_4 productivity after removal of H_2O and O_2 from the feed gas in the last cycles 21–30 (Fig. 4 and S5c). Thus, the stable cyclic performance of (3%Ru)10%Ba/Al at a very low temperature of 250°C qualified this material as highly promising for cyclic CO_2 capture from diluted source and subsequent conversion to concentrated CH_4 even in the presence of H_2O and O_2. Catalyst with relevant methanation kinetics at low temperatures are highly desired for the energetic sustainability of the process, especially for direct air capture (DAC) application in which very large gas volume should flow through the DFM and be heated from room temperature to the desired temperature. Regarding energy consumption in regeneration step of DFM, no external supply of heat is necessary because the temperature is sustained by the heat generated by the exergonic methanation reaction. For processes that capture and regeneration are performed using two different materials in contrast to DFM, the regeneration is very energy intensive and makes the process uneconomic [37–39]. Although the CH_4 concentration in the gas in our experiment is low (lower than 0.01%) for analysis purposes, it can be increased in practice. To this end, only increasing the ratio of DFM material to gas flow rate would be necessary as demonstrated in the literature [13]. For the validation of the materials under industrially relevant conditions, it is important to perform long-term aging studies using a real flue gas (containing O_2 and water vapour) and the scale up of the process. Our results show that H_2O compete with CO_2 for the alkaline capture sites reducing the capture capacity and it is not clear how this will affect in the longer term and with variations of humidity. On the other hand, O_2 can partially oxidise the noble metal. However, it is reported that Ru reduces readily when exposed again to H_2 atmosphere [29,40]. Some authors found deactivation of low loading Ru (<1 wt%) in the presence of O_2 due to the loss of active surface area by Ru sintering. These authors also mentioned that the deactivation is less severe for higher loadings as is our case [34]. Elsewhere, aging study of similar DFMs was performed with simulated flue and the performance was stable [29].

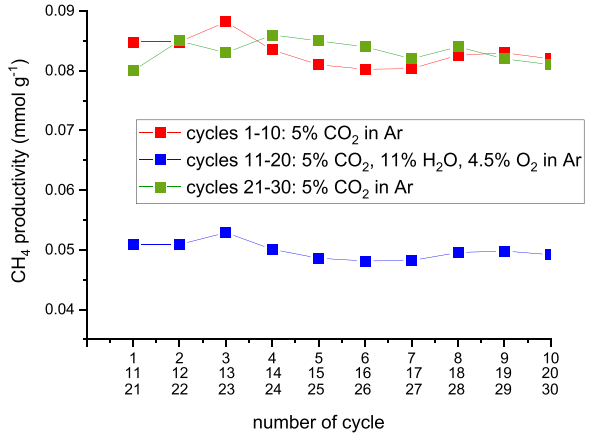

Fig. 4. CH_4 productivity in CO_2 capture and conversion at 250 °C using (3%Ru) 10%Ba/Al material: (red) cycles 1–10, feeding 5% CO_2 in Ar for the capture step; (blue) cycles 11–20, feeding 5% CO_2, 11% H_2O, 4.5% O_2 in Ar for the capture step; (green) cycles 21–30, feeding 5% CO_2 in Ar for the capture step.

The carbon content of the DFMs after the last cycle was analysed by elemental analysis. This carbon accounts for carbon species accumulated in the DFMs during all the CO_2 captured cycles that has not been released in regeneration step under H_2. Generally speaking, the retained carbon decays as temperature increases. It is apparent that some CO_2 is irreversibly captured (accumulated carbon). The amount of carbon irreversible adsorbed decreases when increasing the temperature. Accordingly, a higher proportion of the capture capacity is restored for the subsequent cycle. At the lower temperatures (250 and 300 °C), the amount of irreversibly adsorbed CO_2 is significantly lower for Ba containing DFM than for the other alkaline containing DFMs. For Ba containing material, at the lower temperatures some CO_2 is capture in all the cycles, which is subsequently released as CH_4 keeping a stable cyclic performance.

3.2. *Characterization of the reactivity of COx ad-species by transient techniques*

To assess the CO_2 capture capacity of the dual functional materials, we performed temperature programmed reaction after chemisorption of CO_2 at 300 °C (CO_2-TPD) shown in Fig. 6a. The CO_2 desorption profile exhibited two peaks, one at lower temperature around 100 °C and a second at higher temperature around 350 °C. The first corresponds to physisorbed CO_2 while the second is chemisorbed CO_2. We have no clear explanation for the physisorbed CO_2 since the adsorption was carried out at higher temperature and physisorbed CO_2 should have been removed. It could be attributed to some residual CO_2 present when cooling in Ar. The amount of total desorbed CO_2 follows this increasing order: no alkaline<Ba<Na<K. Therefore, the presence of the alkaline favours the CO_2 capture and the type alkaline follow the same sequence as when they are ordered as a function of the maximum CH_4 productivity, although corresponding to different operation temperatures (Fig. 3), i.e. K (0.48 mmol g^{-1} at 400 °C) <Na (0.41 mmol g^{-1} at 350 °C) < Ba (0.28 mmol g^{-1} at 300 °C).

The reactivity of the different materials towards hydrogenation of adsorbed CO_2 was assessed by TPSR (Fig. 6b-d). To this end, the CO_2 that was previously adsorbed at 50°C is allowed to react with a H_2 flowing gas while heating up to 500 °C at a rate of 10 °C/min. Synchronously, released CO_2, CH_4 and CO gases are monitored by mass spectrometry. At the lowest temperatures, only physisorbed CO_2 evolves because the methanation kinetics are too slow at low temperatures (Fig. 6b). After reaching a certain temperature, CO_2 decays coinciding with the onset of CH_4 and CO, Fig. 5c and 5d, respectively. The trace of CH_4 (Fig. 6c) is around 10-times more intense than that of CO (Fig. 6d), in line with the high selectivity of these materials to CH_4. In the case of (3%Ru)10%Ba/Al, no CO was peak was observed, thus this catalyst being the most selective to CH_4 at low temperatures (Fig. 5) Moreover, CO peak also evolves at lower temperatures than CH_4 peak suggesting that CO is an

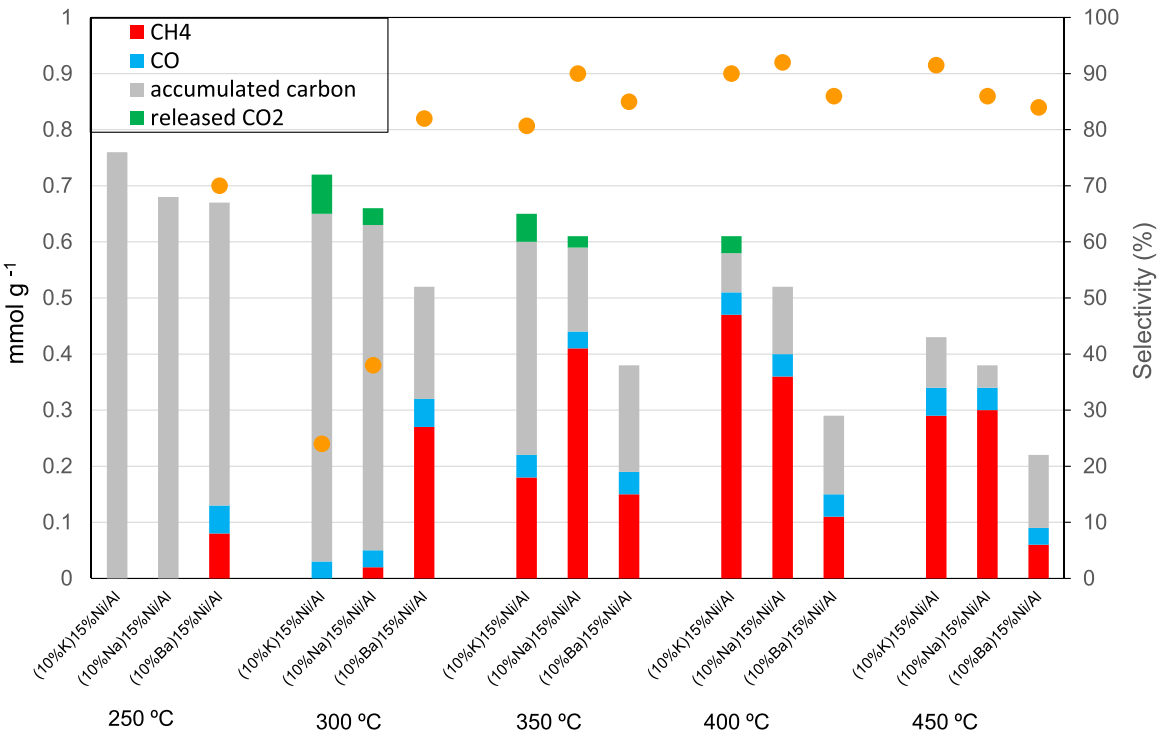

Fig. 5. Carbon balance, CH_4 and CO productivity and selectivity in the last cycle. Accumulated carbon is measured by elemental analysis in the last cycle.

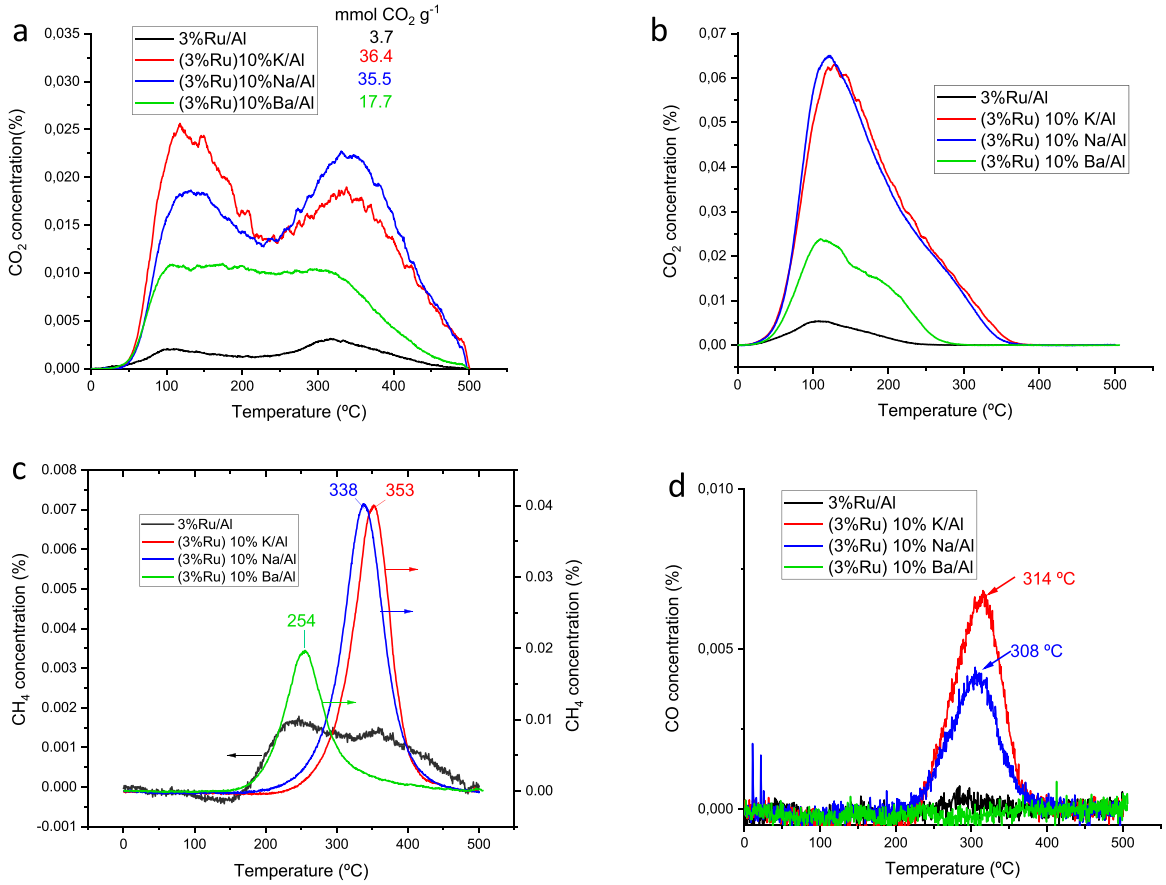

Fig. 6. Characterisation by CO_2-TPD (a) and TPSR (b,c,d) for DFM. (a) CO_2 trace in CO_2-TPD experiment; (b) CO_2 trace in TPSR experiment; (c) CH_4 trace in TPSR experiment; (d) CO trace in TPSR experiment.

intermediate for CH_4 formation. In first step CO_2 is hydrogenated to CO by r-WGS and later CO is hydrogenated to produce CH_4. It is important to note that TPSR experiments (Fig. 6) and cyclic test (Fig. 3) are fundamentally different type of experiments leading to different selectivities. The temperature is dynamic and static in TPSR and cyclic test, respectively. In addition, CO_2 is adsorbed at room temperature and at high temperature (>250 ºC) in TPSR and cyclic test, respectively, which leads to different CO_x ad-species and subsequent selectivities. However, TPSR gives insight about the reactivity of COx species adsorbed at quasi-room temperature and allows the comparison of CO_2-alkaline adsorption strength for the different base metals.

The monometallic 3%Ru/Al_2O_3 catalyst exhibits a broader and weaker CH_4 peak (Fig. 6c left axis) due to the much lower amount of CO_2 captured than for the alkaline metal containing materials (Fig. 6 right axis). The CH_4 peak for (3%Ru)10%Ba/Al displayed the maximum at 254 ºC with the onset at ~160 ºC. These temperatures were ca. 100 ºC lower than those corresponding to the CH_4 peaks for the materials containing the alkaline metals (K, Na). This indicates that (3%Ru)10% Ba/Al is more active, catalysing methanation at lower temperatures. Consequently, the strength of the bond between the COx ad-species and BaO is weaker and it is readily regenerated at lower temperatures than for the alkaline-containing materials. The lowest CH_4 peak temperature in TPSR found for (3%Ru)10%Ba/Al at 254 ºC could explain its stable performance in cyclic tests at 250 ºC (Fig. 4) and 300ºC (Fig. 1). In contrast, the CH_4 peak temperature for K and Na containing material, occurring at 353 ºC and 338 ºC, respectively, with onset at around 250 ºC agrees with the results of cyclic tests, in which these materials do not produce any appreciable amount of CH_4 at 250 ºC and the cyclic performance degrades at 300 ºC losing CO_2 capacity with the number of cycles (Fig. 1).

3.3. Ex-situ characterization of the materials

The materials before reaction were characterized by XEDS-mapping in STEM mode (Fig. 7 and Figs. S6, S7 of supplementary information). As a representative example, Fig. 7 shows the XEDS-mapping for (3%Ru) 10%Ba/Al material. The mappings for all the materials show that both the base metal (Ba, K, and Na) and Ru nanoparticles are distributed throughout all the alumina surface. This guaranties the proximity between both functions, which is a requisite for the synergistic operation of the dual functional materials. In one place, a high local concentration of Ba is found indicating some clustering,

In the XRD diffractograms of used materials (Fig. 8), the more intense diffraction peaks correspond to the (400) and (440) phases of γ-alumina (PDF 04–0858). The XRD pattern showed the formation of Ru nanoparticles as indicated by Ru (101) and (103) planes at 2θ values of 44.0° and 78.1° (PDF 70–0274). The presence of reduced Ru agrees with the preparation procedure which includes a final step of reduction in H_2 at 500 ºC. Ru can oxidise upon re-exposition to air but RuO_2 with the main diffraction peak at 28.0° (110) (PDF 431027) is not visible in the diffractograms suggesting that RuO_2 is amorphous or very small layer. For (3%Ru)10%Ba/Al, the sharp diffraction peaks at 23.9º and 34 º can be also assigned to (111) and (211) crystal phases of barium oxides (PDF 03–0306). For (3%Ru)10%K/Al, the characteristic peak of K_2O at 31.6º (PDF 16–0820) was observed. For (3%Ru)10%Na/Al, the sharp peaks at 32 º can be ascribed to Na_2O (PDF 65–2978) [41,42].

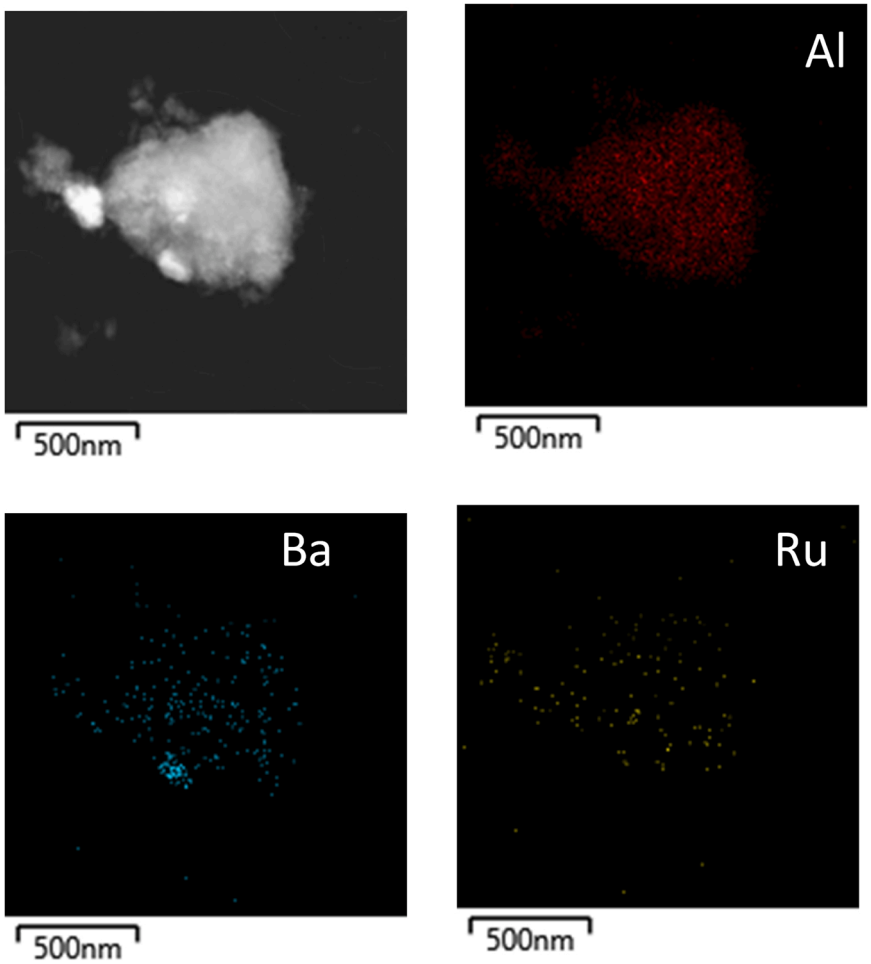

Fig. 7. XEDS-mapping in STEM mode for the used (3%Ru)10%Ba/Al material.

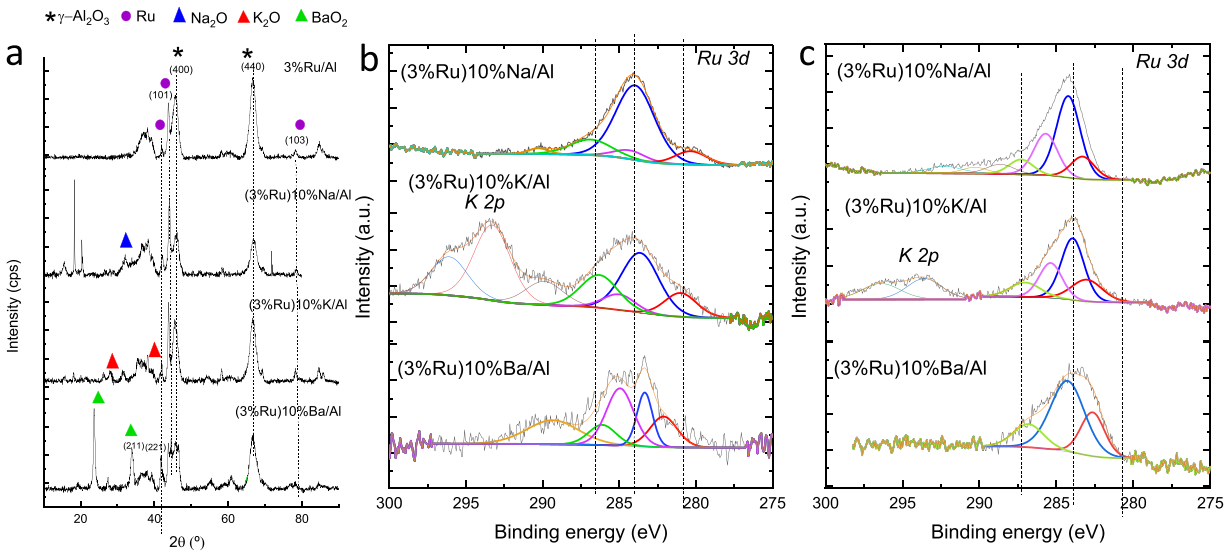

Fig. 8. Characterization of DFMs materials: (a) X-ray diffraction peaks for monometallic and bimetallic catalysts before use; (b) X-ray photoelectron Ru 3d core level spectra of *ex-situ* reduced DFMs before reaction; (c) X-ray photoelectron Ru 3d core level spectra of DFMs after the step of CO_2 capture.

Figs. 8b and 8c show the Ru 3d XPS core level spectra of the as-prepared materials (*ex-situ* reduced at 500 ºC in H_2 and passivated at atmospheric conditions) and of DFMs after the step of reaction with CO_2, respectively. The K-containing material displays also an overlapping peak at higher binding energies which corresponds to K 2p core level. The Ru $3d_{5/2}$ peaks at 280.3 eV and 280.9 eV are generally attributed to Ruº[43] and RuO_2,[44] respectively. A peak of Ru $3d_{5/2}$ spectrum at 282.2 eV is assigned to Ru of oxidation state higher than IV^+ such as Ru oxyhydroxide [45]. Above 283 eV is difficult to assign the Ru 3d peak because they overlap with the C 1 s peak at 284.6 eV. It is important to note that the C 1 s peak (blue line in Fig. 8b and c) must come from carbonated species and it is present both in reduced and used materials. In the *ex-situ* reduced samples, the presence of the peak of C 1 s at 284.6 eV indicates that CO_2 is adsorbed from the atmosphere even at room temperature [46]. Therefore, for the study of Ru species, we have focused on the contributions below 283 eV. The position of the peak corresponding to the more reduced species (red peak corresponding to either Ruº or RuO_2) along with the Ru/Al ratios are listed in Table 1. Among the *ex-situ* reduced DFMs, the Ba-containing one exhibited a shift towards more oxidised species, suggesting an electron-withdrawing effect of Ba over Ru which may also explain its enhanced performance. In contrast, Na apparently exerts a slight electron donating effect. After reaction with CO_2 (Fig. 8c), the peak of the most reduced species (Ruº and RuO_2) vanished or shifted to higher binding energies for all the materials. This is in line with either the oxidation of Ru (oxidation state $> IV^+$) during CO_2 cycle or that the carbonated species have an electro-withdrawing effect. Regarding the Ru/Al ratio determined by XPS (Table S1), the absolute values must be taken with caution because XPS probes only the outermost surface Ru species. However, some conclusions can be derived from relative variations. Compared to the monometallic 3%Ru/Al catalyst, the Ru/Al ratio decreases in the reduced bimetallic catalysts which can be due to a certain Ru masking by the alkaline metal. After formation of the carbonated species in the used catalysts, Ru is apparently segregated to the surface, increasing the Ru/Al ratio. The Al/O atomic ratio for the monometallic catalyst is close to the stoichiometric of Al_2O_3 (0.66). The ratio decreases when adding the alkaline in the bimetallic materials, which can be explained by the increase of oxygen content due to the alkaline oxide formation. The Al/O decreases further after reaction with CO_2, possibly due to increase of oxygen content due to the formation of the alkaline carbonated species and the oxidation of Ru. In summary, the main conclusion of XPS characterization is that Ru and base metals undergoes some redox changes during cycling between reduced species and oxidized states.

We performed a carbon balance in the las cycle for each material and temperature (Table S2 of supplementary material). The captured CO_2 was estimated by analysing the carbon content of the sample after capture step by elemental analysis. It is apparent that the captured CO_2 decreases when temperature increases. The opposite trend is observed for the unreacted carbon suggesting that stable carbon-containing species are retained at the lower temperatures. The cyclic testing and the characterisation of the materials lead us to propose the following mechanism (Fig. 9). During CO_2 feeding, CO_2 is captured by dissociative adsorption on Ru nanoparticles and on basic sites of Al_2O_3 support and by alkaline metal (step 1 of Fig. 9). Concomitantly, Ru is partially oxidised and CO and H_2O are released to atmosphere. In the next step of H_2-feeding, a complex multistep process occurs. First, the partially oxidised noble metal is reduced (step 2 of Fig. 9). Subsequently, CH_4 and CO evolve via two different mechanisms (step 3 of Fig. 9). One route (yellow arrows) is the reduction of the CO_x ad-species captured on the alkaline metal or alumina support mediated by spill-over of H_2 dissociatively chemisorbed on the catalyst surface.[15,47] Other co-operating mechanism also suggested in the literature (green arrows) [16,17,31] is that the heat generated by the exothermicity of methanation may trigger the thermal desorption of adsorbed CO_2, which is transported to Ru sites and reduced thanks to chemisorbed -H on Ru. In the process, the structure/composition of DFM undergoes some dynamic changes which lead to the regeneration of the material for next cycle. The kinetics of reduction and regeneration of the capture material depends mainly on the type of alkaline metal and on the temperature. In the case of Ba containing material, the kinetics of reduction are revealed faster by TPSR experiments and the catalyst is properly regenerated even at low temperature (Fig. 9 step 4 left). In contrast, the slower reduction kinetics for the other alkali metals makes that the alkaline is not completely reduced/regenerated for next cycle at temperatures < 350 ºC. Although the slower kinetics of Na-based DFM makes that material is not properly regenerated at 300 ºC under our reaction conditions (Figs. 1 and 3a and c), stable cyclic performance could be obtained by increasing the methanation time and H_2 concentration. In fact, stable cyclic performance has been attained during 50 cycles with similar material (5%Ru-6% Na on Al_2O_3)[29] at 300 ºC by using 15 min and 15% H_2 in the methanation step. The optimization of H_2 concentration and time will be addressed in future works. The faster kinetics of Ba can be attributed to several factors such as the higher reducibility of COx ad-species or promoting effects (geometric or electronic) of the alkaline on the Ru metal catalyst.[48] To

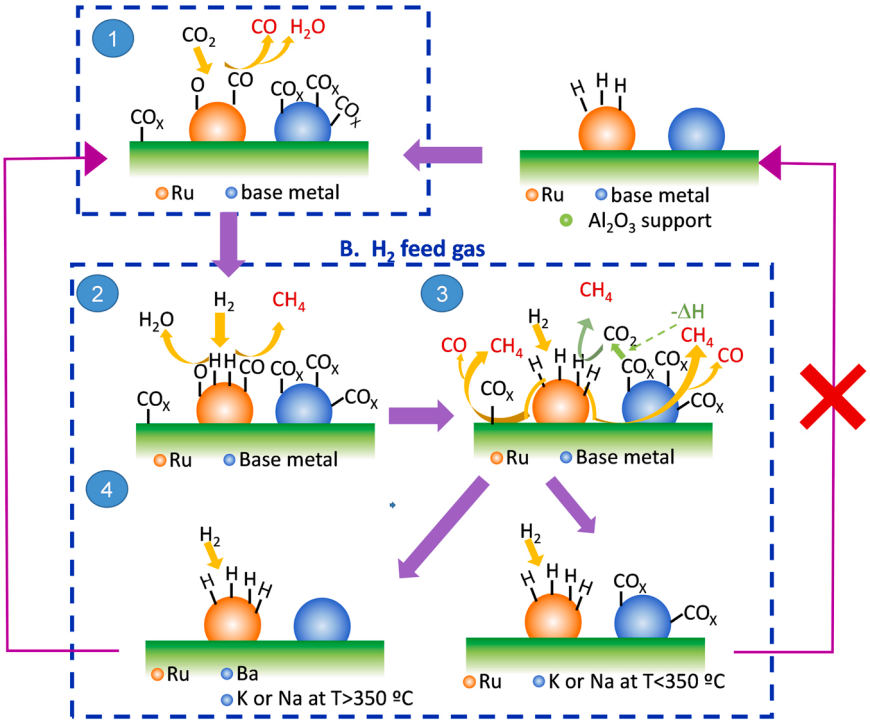

Fig. 9. Schematic representation of the proposed reaction mechanism.

unravel the exact reasons of the different behaviour for each metal, studies by in-situ or operando FTIR spectroscopy[22] must be very helpful in future research. Other matter that should be researched is to design the catalyst to make it even more selective to CH_4 avoiding the release of CO traces.

4. Conclusions

The concept of "dual functional material" has excellent prospects for capturing CO_2 from diluted feeds, like post-combustion flue gas or direct air capture, and subsequently reduce it to CH_4. The integration of both capture and conversion in one single reactor and using only one single homogeneous material entails significant benefits in terms of process intensification. Herein, the cyclic stability of dual functional materials consisting of Ru as methanation catalyst and an alkali metal (K or Na) or alkaline-earth metal (Ba) as CO_2 capture materials has been assessed. While K and Na have been widely used in DFMs, heavy alkaline earth metals such as Ba material have been rarely used. Each material exhibited a different temperature window where CH_4 productivity is maximized, namely, the highest temperature for K-containing DFM (ca. 400 ºC), intermediate temperature for Na-containing DFM (ca. 350 ºC) and the lowest temperature for Ba-containing DFM (<300 ºC). Regarding the cyclic stability, the performance of K and Na based materials at 300 ºC degraded in the first 5 cycles down to zero CH_4 yield. At temperatures of 350 ºC and above, stable cyclic performance was found when using these materials. In contrast, the performance of Ba-containing material at 300 ºC was stable keeping a high value of CH_4 productivity (0.28 ± 0.03 mmol g^{-1}). Moreover, this catalyst afforded a noticeable CH_4 production (0.05–0.08 mmol g^{-1}) and cyclic stability at a temperature as low as 250 ºC and even in the presence of O_2 and H_2O, at which the other DFMs exhibited negligible CH_4 yield. To the best of our knowledge, this is one of the lowest temperatures reported to date for a dual functional material in the CO_2 capture and methanation process. TPSR experiments disclosed that the reason of this behaviour is the enhanced reactivity of the CO_x ad-species for Ba-containing material, which start to react at a temperature as low as 160 ºC. This temperature is more than 50ºC lower than the onset temperature for the reaction of COx ad-species when using K and Na containing materials. The enhanced methanation kinetics affords in turn an adequate regeneration of the material for a subsequent CO_2 capture cycle, leading to a stable cyclic performance. The selectivity to CH_4 is above 80% for the relevant temperatures, being CO an intermediate in CH_4 formation. The characterization of the materials revealed a good distribution of both the methanation and capture functions on the alumina support. XPS of as-prepared DFMs revealed that Ba-containing DFM exhibited the most electron-deficient Ru state among DFMs, which can be on the base of the enhanced performance. This microenvironment created by each base metal would impact on redox dynamics of the two metals and thus on the reactivity of COx ad-species.

Supporting information

Figure S1: Scheme and photograph of the set-up; Fig. S2-S4: Cycles CO_2 capture and conversion using Ru-based catalysts with different alkaline metals at different temperatures 350 ºC, 400 ºC, 450 ºC; Fig. S5: cycles of CO_2 capture and conversion at 250 ºC using (3%Ru)10%Ba/Al; Figs. S6 and S7: XEDS-mapping in STEM mode for (3%Ru)10%K/Al and (3%Ru)10%Na/Al materials, respectively; Table S1: XPS data of catalyst before and after reaction; Table S2: Balance of carbon: CH_4, CO productivity, unreacted CO_2 and carbon capture for the last cycle at different temperatures.

CRediT authorship contribution statement

Enrique García-Bordejé: Conceptualization, Supervision, Writing – original draft preparation. **Ana Belén Dongil:** Investigation, Data curation. **Jorge Moral**: Investigation **José M. Conesa**: Investigation, Data curation. **Antonio Guerrero-Ruiz:** Writing – review & editing. **Inmaculada Rodríguez-Ramos**: Writing – review & and editing.

Declaration of Competing Interest

The authors declare that they have no known competing financial interests or personal relationships that could have appeared to influence

the work reported in this paper.

Data Availability

The authors do not have permission to share data.

Acknowledgements

The Financial support from Spanish Ministry MINECO (projects PID2020-119160RB-C21 and -C22), Gobierno de Aragón (Grupo Reconocido Gobierno de Aragón T03_20R), and associated EU Regional Development Funds are gratefully acknowledged.

Appendix A. Supporting information

Supplementary data associated with this article can be found in the online version at doi:10.1016/j.jcou.2022.102370.

References

[1] P. Friedlingstein, R.M. Andrew, J. Rogelj, G.P. Peters, J.G. Canadell, R. Knutti, G. Luderer, M.R. Raupach, M. Schaeffer, D.P. van Vuuren, C. Le Quéré, Persistent growth of CO_2 emissions and implications for reaching climate targets, Nat. Geosci. 7 (2014) 709–715, https://doi.org/10.1038/ngeo2248.

[2] J. Rogelj, M. den Elzen, N. Höhne, T. Fransen, H. Fekete, H. Winkler, R. Schaeffer, F. Sha, K. Riahi, M. Meinshausen, Paris agreement climate proposals need a boost to keep warming well below 2 °C, Nature 534 (2016) 631–639, https://doi.org/10.1038/nature18307.

[3] C.-H. Yu, C.-H. Huang, C.-S. Tan, A review of CO_2 capture by absorption and adsorption, Aerosol Air Qual. Res. 12 (2012) 745–769, https://doi.org/10.4209/aaqr.2012.05.0132.

[4] C. Song, Q. Liu, N. Ji, S. Deng, J. Zhao, Y. Li, Y. Song, H. Li, Alternative pathways for efficient CO_2 capture by hybrid processes—a review, Renew. Sustain. Energy Rev. 82 (2018) 215–231, https://doi.org/10.1016/j.rser.2017.09.040.

[5] C.R. Müller, P. Abdala Macarena, M. Krödel, A. Landuyt, Mechanistic understanding of CaO-based sorbents for high-temperature CO_2 capture through advanced characterization: recent progress and prospects, ChemSusChem (2020), https://doi.org/10.1002/cssc.202002078.

[6] J. Blamey, E.J. Anthony, J. Wang, P.S. Fennell, The calcium looping cycle for large-scale CO_2 capture, Prog. Energy Combust. Sci. 36 (2010) 260–279, https://doi.org/10.1016/j.pecs.2009.10.001.

[7] P. Melo Bravo, D.P. Debecker, Combining CO_2 capture and catalytic conversion to methane, Waste Dispos. Sustain. Energy 1 (2019) 53–65, https://doi.org/10.1007/s42768-019-00004-0.

[8] K. Ghaib, F.-Z. Ben-Fares, Power-to-methane: a state-of-the-art review, Renew. Sustain. Energy Rev. 81 (2018) 433–446, https://doi.org/10.1016/j.rser.2017.08.004.

[9] J.V. Veselovskaya, P.D. Parunin, O.V. Netskina, A.G. Okunev, A novel process for renewable methane production: combining direct air capture by K2CO3/Alumina sorbent with CO_2 methanation over ru/alumina catalyst, Top. Catal. 61 (2018) 1528–1536, https://doi.org/10.1007/s11244-018-0997-z.

[10] S.J. Park, M.P. Bukhovko, C.W. Jones, Integrated capture and conversion of CO_2 into methane using NaNO3/MgO + Ru/Al2O3 as a catalytic sorbent, Chem. Eng. J. 420 (2021), 130369, https://doi.org/10.1016/j.cej.2021.130369.

[11] J.V. Veselovskaya, P.D. Parunin, O.V. Netskina, L.S. Kibis, A.I. Lysikov, A. G. Okunev, Catalytic methanation of carbon dioxide captured from ambient air, Energy 159 (2018) 766–773, https://doi.org/10.1016/j.energy.2018.06.180.

[12] J.V. Veselovskaya, A.I. Lysikov, O.V. Netskina, D.V. Kuleshov, A.G. Okunev, K2CO3-containing composite sorbents based on thermally modified alumina: synthesis, properties, and potential application in a direct air capture/methanation process, Ind. Eng. Chem. Res. 59 (2020) 7130–7139, https://doi.org/10.1021/acs.iecr.9b05457.

[13] C.V. Miguel, M.A. Soria, A. Mendes, L.M. Madeira, A sorptive reactor for CO_2 capture and conversion to renewable methane, Chem. Eng. J. 322 (2017) 590–602, https://doi.org/10.1016/j.cej.2017.04.024.

[14] C. Jeong-Potter, R. Farrauto, Feasibility study of combining direct air capture of CO_2 and methanation at isothermal conditions with dual function materials, Appl. Catal. B Environ. 282 (2021), 119416, https://doi.org/10.1016/j.apcatb.2020.119416.

[15] H.Y. Kim, H.M. Lee, J.-N. Park, Bifunctional mechanism of CO_2 methanation on Pd-MgO/SiO2 catalyst: independent roles of MgO and Pd on CO_2 methanation, J. Phys. Chem. C. 114 (2010) 7128–7131, https://doi.org/10.1021/jp100938v.

[16] L. Proaño, E. Tello, M.A. Arellano-Trevino, S. Wang, R.J. Farrauto, M. Cobo, In-situ DRIFTS study of two-step CO_2 capture and catalytic methanation over Ru,"Na2O"/Al2O3 dual functional material, Appl. Surf. Sci. 479 (2019) 25–30, https://doi.org/10.1016/j.apsusc.2019.01.281.

[17] A. Bermejo-López, B. Pereda-Ayo, J.A. González-Marcos, J.R. González-Velasco, Mechanism of the CO_2 storage and in situ hydrogenation to CH4. Temperature and adsorbent loading effects over Ru-CaO/Al2O3 and Ru-Na2CO3/Al2O3 catalysts, Appl. Catal. B Environ. 256 (2019), 117845, https://doi.org/10.1016/j.apcatb.2019.117845.

[18] M.S. Duyar, M.A.A. Treviño, R.J. Farrauto, Dual function materials for CO_2 capture and conversion using renewable H2, Appl. Catal. B Environ. 168–169 (2015) 370–376, https://doi.org/10.1016/j.apcatb.2014.12.025.

[19] M.S. Duyar, S. Wang, M.A. Arellano-Treviño, R.J. Farrauto, CO_2 utilization with a novel dual function material (DFM) for capture and catalytic conversion to synthetic natural gas: an update, J. CO_2 Util. 15 (2016) 65–71, https://doi.org/10.1016/j.jcou.2016.05.003.

[20] M.A. Arellano-Treviño, Z. He, M.C. Libby, R.J. Farrauto, Catalysts and adsorbents for CO_2 capture and conversion with dual function materials: limitations of Ni-containing DFMs for flue gas applications, J. CO_2 Util. 31 (2019) 143–151, https://doi.org/10.1016/j.jcou.2019.03.009.

[21] L.F. Bobadilla, J.M. Riesco-García, G. Penelás-Pérez, A. Urakawa, Enabling continuous capture and catalytic conversion of flue gas CO_2 to syngas in one process, J. CO_2 Util. 14 (2016) 106–111, https://doi.org/10.1016/j.jcou.2016.04.003.

[22] T. Hyakutake, W. van Beek, A. Urakawa, Unravelling the nature, evolution and spatial gradients of active species and active sites in the catalyst bed of unpromoted and K/Ba-promoted Cu/Al2O3 during CO_2 capture-reduction, J. Mater. Chem. A 4 (2016) 6878–6885, https://doi.org/10.1039/C5TA09461E.

[23] A. Bermejo-López, B. Pereda-Ayo, J.A. González-Marcos, J.R. González-Velasco, Ni loading effects on dual function materials for capture and in-situ conversion of CO_2 to CH4 using CaO or Na2CO3, J. CO_2 Util. 34 (2019) 576–587, https://doi.org/10.1016/j.jcou.2019.08.011.

[24] F. Kosaka, Y. Liu, S.-Y. Chen, T. Mochizuki, H. Takagi, A. Urakawa, K. Kuramoto, Enhanced activity of integrated CO_2 capture and reduction to CH4 under pressurized conditions toward atmospheric CO_2 utilization, ACS Sustain. Chem. Eng. (2021), https://doi.org/10.1021/acssuschemeng.0c07162.

[25] L. Hu, A. Urakawa, Continuous CO_2 capture and reduction in one process: CO_2 methanation over unpromoted and promoted Ni/ZrO2, J. CO_2 Util. 25 (2018) 323–329, https://doi.org/10.1016/j.jcou.2018.03.013.

[26] S. Cimino, F. Boccia, L. Lisi, Effect of alkali promoters (Li, Na, K) on the performance of Ru/Al2O3 catalysts for CO_2 capture and hydrogenation to methane, J. CO_2 Util. 37 (2020) 195–203, https://doi.org/10.1016/j.jcou.2019.12.010.

[27] J.V. Veselovskaya, P.D. Parunin, A.G. Okunev, Catalytic process for methane production from atmospheric carbon dioxide utilizing renewable energy, Catal. Today 298 (2017) 117–123, https://doi.org/10.1016/j.cattod.2017.05.044.

[28] Q. Zheng, R. Farrauto, A. Chau Nguyen, Adsorption and methanation of flue gas CO_2 with dual functional catalytic materials: a parametric study, Ind. Eng. Chem. Res. 55 (2016) 6768–6776, https://doi.org/10.1021/acs.iecr.6b01275.

[29] S. Wang, R.J. Farrauto, S. Karp, J.H. Jeon, E.T. Schrunk, Parametric, cyclic aging and characterization studies for CO_2 capture from flue gas and catalytic conversion to synthetic natural gas using a dual functional material (DFM), J. CO_2 Util. 27 (2018) 390–397, https://doi.org/10.1016/j.jcou.2018.08.012.

[30] K.H. Chai, L.K. Leong, D.S.-H. Wong, D.-H. Tsai, S. Sethupathi, Effect of CO_2 adsorbents on the Ni-based dual-function materials for CO_2 capturing and in situ methanation, J. Chin. Chem. Soc. 67 (2020) 998–1008, https://doi.org/10.1002/jccs.202000086.

[31] A. Porta, C.G. Visconti, L. Castoldi, R. Matarrese, C. Jeong-Potter, R. Farrauto, L. Lietti, Ru-Ba synergistic effect in dual functioning materials for cyclic CO_2 capture and methanation, Appl. Catal. B Environ. 283 (2021), 119654, https://doi.org/10.1016/j.apcatb.2020.119654.

[32] A. Porta, R. Matarrese, C.G. Visconti, L. Castoldi, L. Lietti, Storage material effects on the performance of Ru-based CO_2 capture and methanation dual functioning materials, Ind. Eng. Chem. Res. 60 (2021) 6706–6718, https://doi.org/10.1021/acs.iecr.0c05898.

[33] H. Sun, Y. Zhang, S. Guan, J. Huang, C. Wu, Direct and highly selective conversion of captured CO_2 into methane through integrated carbon capture and utilization over dual functional materials, J. CO_2 Util. 38 (2020) 262–272, https://doi.org/10.1016/j.jcou.2020.02.001.

[34] C. Jeong-Potter, A. Porta, R. Matarrese, C.G. Visconti, L. Lietti, R. Farrauto, Aging study of low Ru loading dual function materials (DFM) for combined power plant effluent CO_2 capture and methanation, Appl. Catal. B Environ. 310 (2022), 121294, https://doi.org/10.1016/j.apcatb.2022.121294.

[35] R.J. Berger, J. Pérez-Ramírez, F. Kapteijn, J.A. Moulijn, Catalyst performance testing: bed dilution revisited, Chem. Eng. Sci. 57 (2002) 4921–4932, https://doi.org/10.1016/S0009-2509(02)00273-7.

[36] A. Tsuneto, A. Kudo, N. Saito, T. Sakata, Hydrogenation of solid state carbonates, Chem. Lett. 21 (1992) 831–834, https://doi.org/10.1246/cl.1992.831.

[37] C.W. Jones, CO_2 capture from dilute gases as a component of modern global carbon management, Annu. Rev. Chem. Biomol. Eng. 2 (2011) 31–52, https://doi.org/10.1146/annurev-chembioeng-061010-114252.

[38] E.S. Sanz-Pérez, C.R. Murdock, S.A. Didas, C.W. Jones, Direct capture of CO_2 from ambient air, Chem. Rev. 116 (2016) 11840–11876, https://doi.org/10.1021/acs.chemrev.6b00173.

[39] C.M. Jens, L. Müller, K. Leonhard, A. Bardow, To integrate or not to integrate—techno-economic and life cycle assessment of CO_2 capture and conversion to methyl formate using methanol, ACS Sustain. Chem. Eng. 7 (2019) 12270–12280, https://doi.org/10.1021/acssuschemeng.9b01603.

[40] M.A. Arellano-Treviño, N. Kanani, C.W. Jeong-Potter, R.J. Farrauto, Bimetallic catalysts for CO_2 capture and hydrogenation at simulated flue gas conditions, Chem. Eng. J. 375 (2019), 121953, https://doi.org/10.1016/j.cej.2019.121953.

[41] X. Wu, Y. Zhang, J. Zhang, R. Liu, J. Yang, B. Yang, H. Xu, Y. Ma, High pressure X-ray diffraction study of sodium oxide (Na2O): Observations of amorphization and

equation of state measurements to 15.9 GPa, J. Alloy. Compd. 823 (2020), 153793, https://doi.org/10.1016/j.jallcom.2020.153793.
[42] P. Hartmann, C.L. Bender, J. Sann, A.K. Dürr, M. Jansen, J. Janek, P. Adelhelm, A comprehensive study on the cell chemistry of the sodium superoxide (NaO2) battery, Phys. Chem. Chem. Phys. 15 (2013) 11661–11672, https://doi.org/10.1039/C3CP50930C.
[43] A. Foelske, O. Barbieri, M. Hahn, R. Kötz, An X-ray photoelectron spectroscopy study of hydrous ruthenium oxide powders with various water contents for supercapacitors, Electrochem. Solid-State Lett. 9 (2006) A268, https://doi.org/10.1149/1.2188078.
[44] G. Wang, C.-S. Hsieh, D.-S. Tsai, R.-S. Chen, Y.-S. Huang, Area-selective growth of ruthenium dioxide nanorods on LiNbO3(100) and Zn/Si substrates, J. Mater. Chem. 14 (2004) 3503–3508, https://doi.org/10.1039/B409283J.
[45] H. Over, A.P. Seitsonen, E. Lundgren, M. Smedh, J.N. Andersen, On the origin of the Ru-3d5/2 satellite feature from RuO2(110), Surf. Sci. 504 (2002) L196–L200, https://doi.org/10.1016/S0039-6028(01)01979-3.
[46] M. Cuéllar-Cruz, D.K. Schneider, V. Stojanoff, S.R. Islas, N. Sánchez-Puig, R. Arreguín-Espinosa, J.M. Delgado, A. Moreno, Formation of crystalline silica–carbonate biomorphs of alkaline earth metals (Ca, Ba, Sr) from ambient to low temperatures: chemical implications during the primitive earth's life, Cryst. Growth Des. 20 (2020) 1186–1195, https://doi.org/10.1021/acs.cgd.9b01473.
[47] J.-N. Park, E.W. McFarland, A highly dispersed Pd–Mg/SiO2 catalyst active for methanation of CO_2, J. Catal. 266 (2009) 92–97, https://doi.org/10.1016/j.jcat.2009.05.018.
[48] T.K. Campbell, J.L. Falconer, Carbon dioxide hydrogenation on potassium-promoted nickel catalysts, Appl. Catal. 50 (1989) 189–197, https://doi.org/10.1016/S0166-9834(00)80835-0.